 doi:10.20944/preprints202211.0459.v1

Article

Determination of Optimum Outlet Slit Thickness and Outlet Angle For The Bladeless Fan Using CFD Approach

Vedant Joshi [1], Wedyn Noronha [1], Vinayagamurthy G [2]* and Sivakumar R [1] and Rajasekarababu KB [3]

1 School of Mechanical Engineering, Vellore Institute of Technology, Chennai, India ;
2 Centre for Innovation and Product Development and School of Mechanical Engineering, Vellore Institute of Technology, Chennai, India
3 School of Civil and Environmental Engineering, AIWE- Lab, Harbin Institute of Technology Shenzhen, China
* Correspondence: vinayagamurthy.g@vit.ac.in

Abstract: Toshiba devised the bladeless fan (or Air Multiplier) concept in 1981. Researchers like James Dyson and Jafari et al. further developed it. Bladeless fans are more energy-efficient, safer due to the hidden blades, easier to clean, and more adjustable than conventional fans. From a performance point of view, bladeless fans are better because they multiply mass flow rate, eliminate buffeting, consume less power, and are quieter. This paper investigates the influence of the airfoil's outlet slit thickness on the discharge ratio by varying the outlet slit thickness of an Eppler 473 airfoil from 1.2 mm to 2 mm in intervals of 0.2 mm. Results indicated that smaller slits showed higher discharge ratios. The airfoil with a 1.2 mm slit thickness showed a discharge ratio of 18.78, a 24% increase from the discharge ratio of the 2 mm slit. The effect of outlet angle on the pressure drop across the airfoil was also studied. Outlet angles were varied from 16° to 26° by an interval of 2°. The airfoil profile with a 24° outlet angle showed a maximum pressure difference of 965 Pa between the slit and leading edge. In contrast, the 16° outlet angle showed the least pressure difference of 355 Pa. Parameters such as average velocity, turbulent kinetic energy, the standard deviation of velocity and outlet velocity magnitude was used to assess the performance of airfoil profiles used in bladeless fan.

Keywords: Bladeless fan; Discharge ratio; Coanda effect; Eppler 473; Velocity contour; CFD

1. Introduction

Fans (axial and radial) are used for various applications such as; cooling systems, air conditioning, and ventilation in tunnels and underground spaces. The performance of fans has been enhanced by increasing developments in Computational Fluid Dynamics (CFD) and commercial growth, offering different types of fans with various applications and higher efficacy. The main differences between bladeless and traditional fans are the increasing airflow intake and lack of a visible impeller. A bladeless fan consists of two main sections; the base houses the impeller has vents to suck in air from the surroundings, and passes it through the toroidal section with an airfoil profile, as shown in Figure 1. [1] Demonstrated the working of the bladeless fan. Two phenomena responsible for airflow rate multiplication are the Coanda effect and entrainment.

The Coanda effect at the airfoil creates a pressure difference between the two sides of the fan. Air near the leading edge has a lower pressure, while air near the trailing edge has higher pressure. Due to the pressure difference, more air is blown from the leading edge to the trailing edge. Entrainment occurs at the inlet (near the toroidal section) and outlet of the fan. It then passes by the toroidal section, exits from the outlet slit, and multiplies mass flow rates across their ends, improving the outlet velocity. Entrainment sucks in air at the fan's base and from the back of the fan. The entrainment and multiplication of airflow increases the efficiency of the fan.

Theoretically, discharge ratio is the ratio of the fan's outlet velocity to the inlet velocity, which is influenced by several factors, such as the outlet slit thickness of the airfoil, the angle of outlet flow relative to the fan's axis, the height of the fan cross-section, the aspect ratio of fan cross-section, the hydraulic diameter of the fan according to studies conducted by [2]. The major parameters such as outlet slit thickness and outlet slit angle are directly

 doi:10.20944/preprints202211.0459.v1

concerned with the flow passage and thus the quthor persumes that these parameters has major influence on performance of bladeless fan. In the current work, a preliminary study on a 2-dimensional bladeless fan was conducted to understand the flow behaviour when the slit thickness was varied. A three-dimensional analysis assesses the effect of slit thickness and outlet angle.

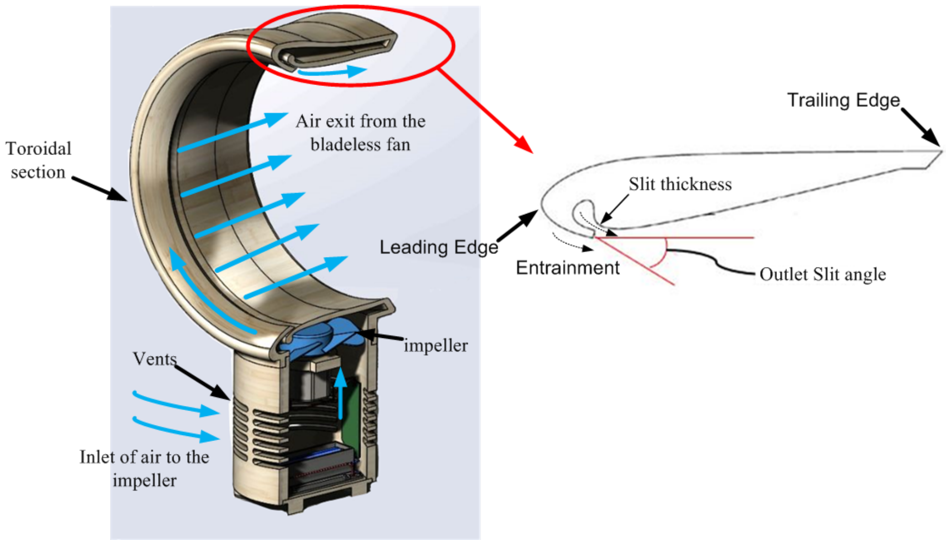

Figure 1. Eppler 473 Airfoil Profile with the depiction of outlet slit and height of cross-section.

2. Literature Survey

Very few studies have been conducted on Bladeless fans using CFD. [2,3] Conducted an experimental and numerical analysis on bladeless fans by changing parameters such as the fan cross-section height, flow outlet angle relative to the fan axis, hydraulic diameter, and aspect ratio. CFD analysis identified that the discharge ratio is maximum for a cross-sectional height of 3 cm and an outlet angle of 16°. For aspect ratios greater than 1, the discharge ratio decreases considerably. All profiles in the present study have an aspect ratio equal to 1.

A parabolic velocity profile is ideal for cooling since the maximum velocity is at the centre. Figure 2(a) shows an axial fan blast profile, where the velocity is maximum near the edges and reduces at the axis. Jet equations cannot determine the target distance for axial cooling fans. Still, they can be used for bladeless fans since the velocity profile of the output of bladeless fans is parabolic, Figure 2 (b).

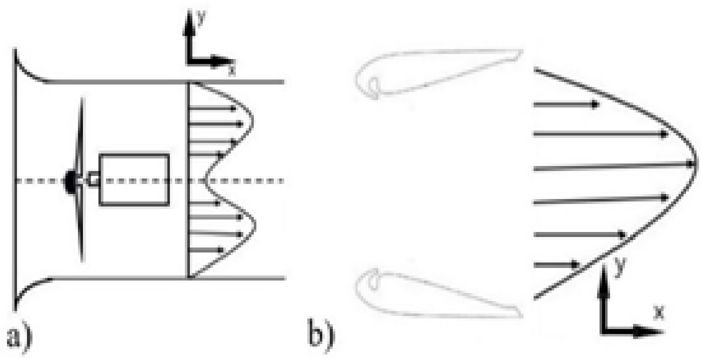

Figure 2. Eppler 473 Airfoil Profile with the depiction of outlet slit and height of cross-section.

The acoustic and aerodynamic performances of fans are the two major advantages of the Bladeless. Bladeless fans are generally quieter than conventional fans owing to their elimination of buffeting. The bladeless fan output is uniform and has the maximum

Preprints (www.preprints.org) | NOT PEER-REVIEWED | Posted: 24 November 2022 doi:10.20944/preprints202211.0459.v1

velocity at the centre of its velocity profile, optimal for cooling purposes. [2,4] investigated noise levels of a Bladeless fan in steady and unsteady flow conditions, using Broadband Noise Source (BNS) and Ffowcs Williams and Hawkings (FW-H) equations. The numerical investigation indicated that the outlet slit of air is the primary noise source.

Previous researchers have conducted CFD investigations on centrifugal and axial-bladed fans to optimise the mass flow rate and enhance performance. Recently, [5] performed a behavioural study on maximising the number of blades on a radial fan. They reported that the mass flow rate at the outlet increases with the number of blades. Furthermore, they performed a transient three-dimensional analysis of standard ceiling fans. Results showed that the ceiling fan could replace the airflow characteristics generated by the fan's meandering plume and local fine shear layers. [6] performed several simulations to optimise an airfoil profile to enhance mine ventilation fans' efficiency. Out of 6 distinct fan profiles, the NACA 747A315 showed the lowest energy consumption and maximum efficiency.

3. Major Parameters Influencing Bladeless Fan

The major parameters influencing the performance of the bladeless fan such as airfoil profile, outlet thickness, outlet angle and maximum inlet velocity from the impeller are discussed below.

3.1. Airfoil Profile

The airfoil is the primary working surface for energy transfer, and therefore proper airfoil selection is significant. Eppler 473 has higher curvature offering a good Coanda surface, thus providing better suction of air from the back of the fan. The outlet volume flow rate increased linearly with an increase in the inlet volume flow rate. According to [7], noise emissions increase with an increased inlet volume flow rate. [8] Postulated that with increasing curvature of the Coanda surface, several low-pressure regions along the airfoil are gradually enlarged, begin to merge slowly, and finally form a large area of low pressure, thus improving the Coanda effect.

The results of the study by [9] indicate that the overall performances were substantially equivalent. With a drop of 8% of pressure rise at a conception flow rate for the thick blades fan and maximum efficiency that is 3% lower than the efficiency of the thin blades fan and that is shifted towards lower flow rates. The efficiency of thick airfoils is 3% less than that of thin airfoils with low flow rates. The Eppler's discharge ratio of 473 airfoils is highest when the thickness of the cross-section is 3 cm. [10] Declared that thicker blades demand higher power consumption since they add weight to the fan and lead to excess vibration and failure.

3.2. Outlet Slit Thickness

The outlet slit is the gap through which air exits the airfoil profile depicted in Figure 1. The slit thickness is the most influential factor in the discharge ratio. Theoretically, the smaller the slit thickness, the higher the output velocity and the higher the pressure drop, enhancing the Coanda effect.

3.3. Outlet Angle and Velocity

The angle between the horizontal and the normal outlet slit is the outlet angle, refer Figure 1. The outlet slit angle affects the amount of pressure drop across the airfoil and the convergence distance of the velocity profile. In Figure 1 shows the outlet angle of an airfoil profile.The constraint of the environment binds the outlet velocity. Cooling fans usually have outlet velocities between 2 m/s and 7 m/s. Velocities that are too high will be uncomfortable for occupants.

Preprints (www.preprints.org) | NOT PEER-REVIEWED | Posted: 24 November 2022 doi:10.20944/preprints202211.0459.v1

3.4. Maximum Inlet Velocity

[11] Analyzed the exit velocity measurements related to inlet velocity and the wake velocity profile. The inlet velocity increased when the blade passage separation decreased. The wake velocity profile showed uniform velocity distribution when the inlet velocity was higher. This concept from fans with blades can be extrapolated to bladeless fans, increasing velocity by reducing slit thickness.

4. CFD Simulation

In the preliminary study, a two-dimensional analysis was carried out to understand the flow pattern and velocity profile at the exit of the bladeless fan. Two-dimensional analysis has shown that the outlet of the bladeless fan is able to provide uniform velocity, and thus further the study was extended to a three-dimensional analysis to investigate the influence of outlet slit thickness and angle on the performance of the bladeless fan.

4.1. Geometrical modelling

Based on Euler's equations, [12] stated that the energy obtained by the air particles from the fan is directly proportional to the fan's diameter. The fan's diameter was 300 mm in the experimental setup, and the airfoil chord length was 60 mm. In this study, the outlet slit and outlet angles were varied, and flow behaviour was analysed. The outlet slit thickness was varied from 1.2 mm to 2 mm with an interval of 0.2 mm. The outlet angles were varied from 16° to 26° with an interval of 2°.

4.2. Computational Domain and Mesh Generation

The computational domain for the two-dimensional analysis is shown in Figure 3(a); the sidewalls of the domain are 0.65 m apart and are more than twice the fan diameter. The downstream length is 3.1 m, and the total height is 1.6 m. The boundary conditions were; the slow inlet that allows environmental airflow and the inlet through which air from the impeller enters the airfoil. The airfoil profile is set as "walls" and "stationary walls", representing the room's ceiling and floor. The bladeless fan is 1 m from the slow inlet. Figure 3(b) is a magnified illustration of the inlet within the airfoil.

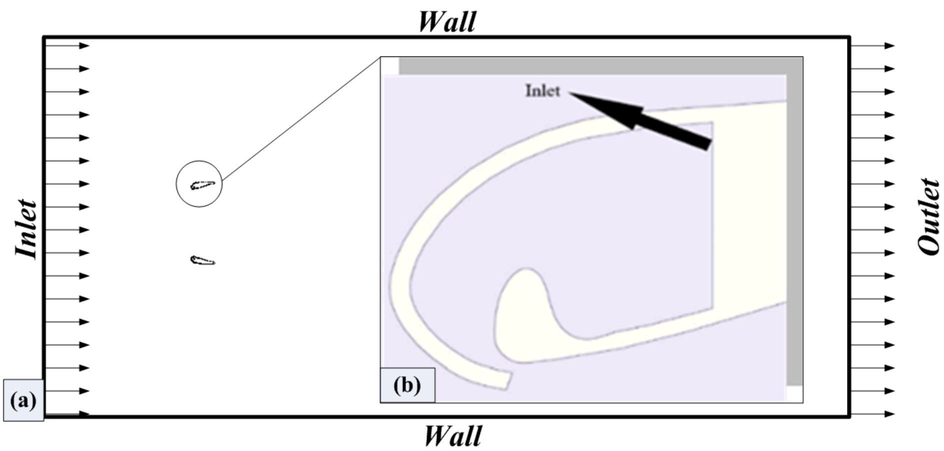

Figure 3. (**a**) Fluid Domain Boundary Conditions. (**b**) Airfoil Boundary condition.

The computational domain was meshed with triangular meshes, with fine inflation layers created around the airfoil to compute the flow features around the blade accurately. A poly-hex core mesh was used, and the total mesh count was nearly 7.1 million. From, Figure 4 (a) shows the fine mesh around the airfoil as a sphere of influence. The y^+ value was set to 1 to capture flow features like pressure, velocity and turbulent kinetic energy near the walls. Figure 4(b) is a zoomed-in view of the inflation layer near the outlet slit region of the airfoil. Twelve inflation layers were generated with a first-layer thickness of 0.03069 mm. The growth rate for the inflation layers was set as 1.05 near the walls.

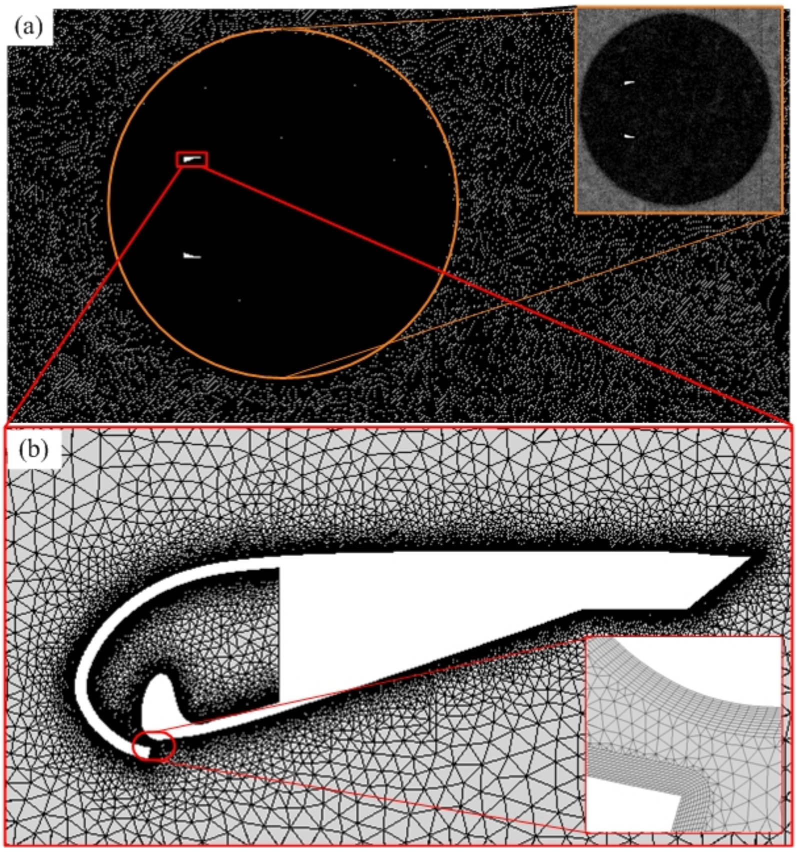

Figure 4. (**a**) 2-D computational domain . (**b**) Inflation layers near airfoil and outlet slit.

The first wall distance was calculated using following equations: Initially, the Reynolds number is calculated to determine whether the flow is laminar or turbulent using Eq. (1).

$$Re = \frac{\rho U L}{\mu} \tag{1}$$

An empirical coefficient for fully developed turbulent flow is then used to estimate the skin friction coefficient. The skin friction coefficient is calculated using Eq. (2), where Re is Reynold's number.

$$c_f = [2log_{10}(Re) - 0.65]^{(-2.3)} \tag{2}$$

Wall shear stress is calculated using Eq.(3), the free stream the velocity (U), density () and skin friction coefficient (C_f).

$$\tau_w = \frac{1}{2}\rho U^2 c_f \tag{3}$$

Now, the Wall shear stress is calculated as shown in Eq. (4).

$$u_T = \sqrt{\frac{\tau_w}{\rho}} \tag{4}$$

Eq. (5) y_p Denotes the distance of the boundary from the centroid of the adjacent cell. The y_p is calculated using the desired y^+ value and friction velocity

$$y_p = \frac{y^+ \mu}{u_T \rho} \tag{5}$$

Finally, using the value of y_p, the first layer thickness is given by Eq. (6), where y_p is the thickness of the first mesh cell from the boundary for inflation layers.

$$y_H = 2y_p \tag{6}$$

From the above equations, the 3D mesh first wall distance is modelled. Figure 5 (a to c) shows aerofoil and volume mesh. The total number of elements was around 15.4 million cells.

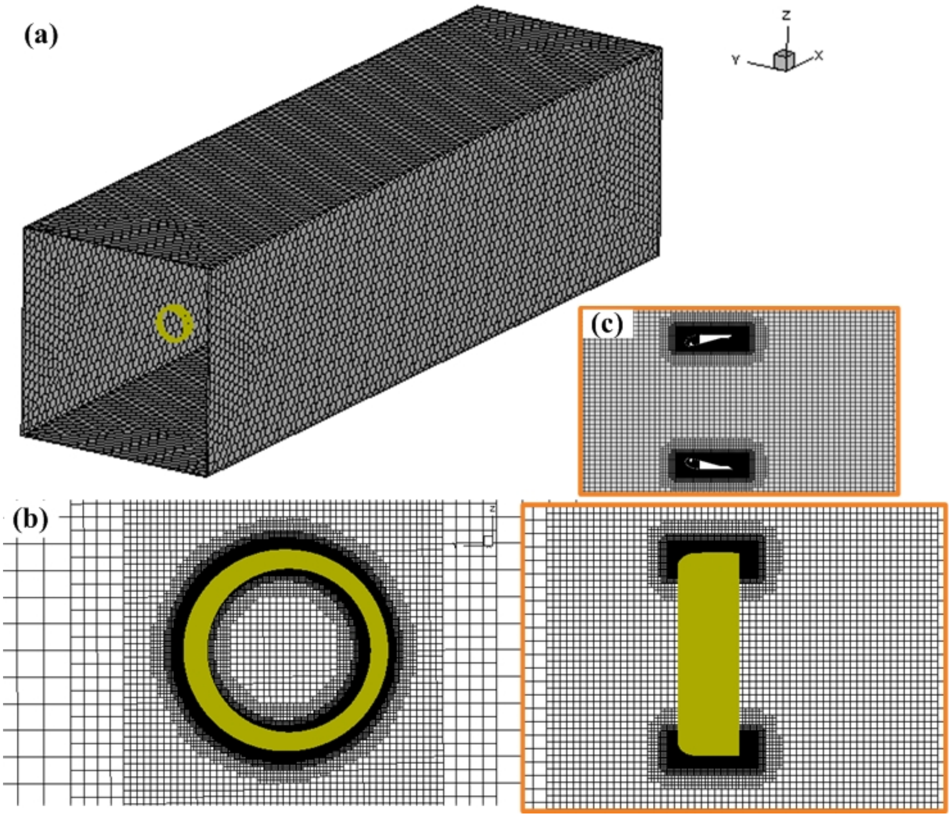

Figure 5. (**a**) 3D Computational domain. (**b**) Bladeless fan mesh zoomed-view .(**c** Inflation layers around the model)

.

4.3. Turbulence model and simulation set-up

The 2-D and 3D simulations are accomplished using a pressure-based solver k-omega SST turbulence model. The k-omega SST turbulence model captures flow features near walls more accurately than other RANS models. A first-layer thickness approach was used to model the inflation layers, which would cover the boundary layers. The equations and formulae required to successfully determine the first layer height based on specific properties like free stream velocity, density, dynamic viscosity, reference length, and adhered y+ value are mentioned in detail. In this simulation, the ambient air velocity was 0.005m/s is fixed. The fan inlet velocity varied from 1 m/s to 6 m/s with an interval of 1 m/s. The outlet was set to standard pressure outlet. The solution was initialised using hybrid initialisation. The residuals of the analysis were selected to 10^{-5} for the continuity, x-velocity, y-velocity, K, and Omega equations.

5. Results and Discussion

5.1. 2D flow analysis of a Bladeless fan

To understand the flow behaviour near the bladeless fan, the results were extracted on various planes (P1, P2, P3, P4, and P5) along with the flow at different distances, as shown in Figure 6. In the defined planes, the flow's velocity profiles were extracted and plotted in Figure 7. In Figure 7 the maximum velocity of 12 m/s at P1 decreases

Preprints (www.preprints.org) | NOT PEER-REVIEWED | Posted: 24 November 2022 doi:10.20944/preprints202211.0459.v1

slowly due to circulation. It is clear from Fig. 7 (a b) that velocity is maximum near the centre and decreases with vertical distance. A significant observation is that the velocity profile becomes constant as the distance from the outlet slit increases. P3 values from both slits (Figure 7) show a substantial peak velocity drop compared with planes 1 and 2. Furthermore, at a distance greater than 0.75 m, the vertical axis velocity profile gradually becomes uniform. Figure 8 (a,b) represents the streamlined flow in the fan's immediate environment.

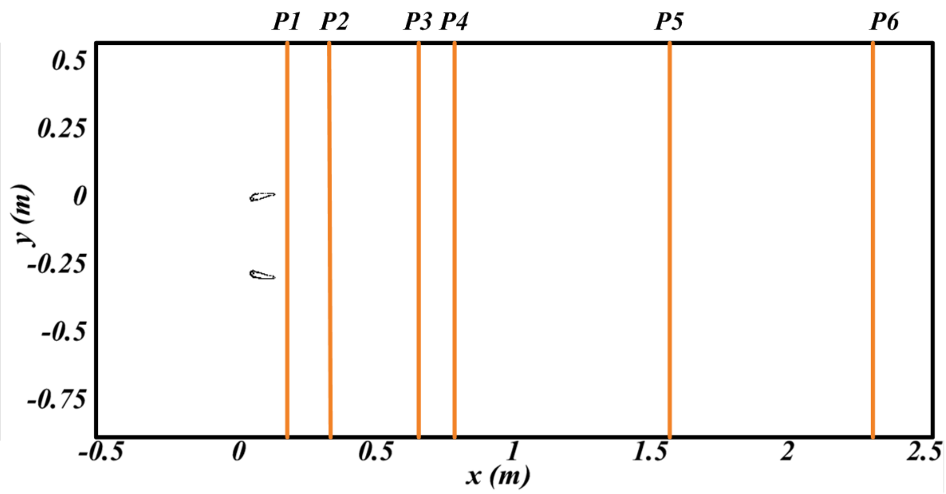

Figure 6. Reference lines in the 2D domain for measuring properties of fluid flow

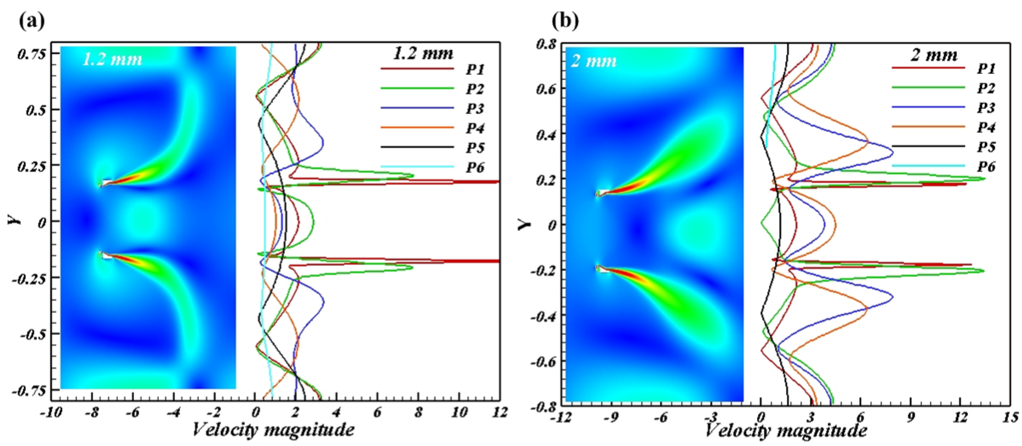

Figure 7. Velocity Profile and contours (**a**) 1.2 mm slit thickness at 3 m/s inlet velocity. (**b**) 2 mm slit thickness at 6 m/s inlet velocity.

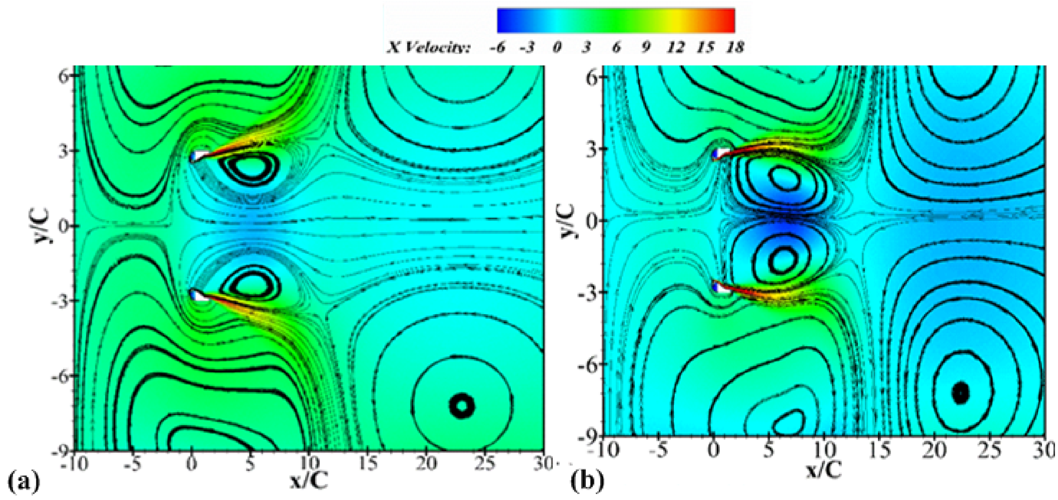

Figure 8. Streamline flow distribution 2-D (**a**) 1.2 mm slit thickness at 3 m/s inlet velocity. (**b**) 2 mm slit thickness at 6 m/s inlet velocity.

5.2. Flow analysis of a Bladeless fan

The 3D- simulations were carried out similarly to the 2-D by varying slit thickness from 1.2 mm to 2 mm and with inlet velocities going from 1 m/s through 6 m/s. The main parameters observed in the 3-dimensional studies were the velocity profile at 0.9 m from the outlet slit, the standard deviation of outlet velocity, turbulent kinetic energy, symmetry of velocity contours, and optimal distance for occupant location. The graphs below compare these parameters from the iterations. In Figure 9(a), the standard deviation of all slits remains almost the same for inlet velocities under 3.3 m/s, and 1.6 mm slit thickness shows the lowest standard deviation up to 5.4 m/s inlet velocity.Figure 9 (b) plots the average velocity in the occupant area versus the inlet velocity. The outlet velocity is similar for all slits when the inlet velocity is below 2.4 m/s; however, beyond 2.4 m/s, the 1.2 mm slit has the highest average outlet velocity. This velocity also falls in the range for occupant comfort. In Figure 9 (c) shows that optimal maximum velocity is attained for 1.2 mm iteration at lower inlet velocities, reducing input power demand. In Figure 9(d), the 2 mm slit thickness had the lowest turbulence kinetic energy.

The inference from the graphs above is that 1.2 mm slit thickness with 3 m/s inlet velocity yields the best results since its outlet velocity is appropriate for usage and its standard deviation is low. Other iterations have comparable velocities, but their inlet velocity is higher, which demands higher power consumption. The iteration with the lowest slit thickness is more energy-efficient to use a change in design rather than increase inlet velocity. The v = 1 m/s iteration showed the least standard deviation, while the v = 6 m/s showed the most significant performance. As the inlet velocity increased, the standard deviation of the velocity outlet also increased. The average of the maximum and minimum of the graph is calculated for the final value of standard deviation. The flow moving away from the trailing edge of the bladeless fan has lower turbulence and a more linear airflow profile than other fans. Airflow with low turbulence travels more efficiently from the emission point and loses less energy and velocity to turbulence than conventional fans.

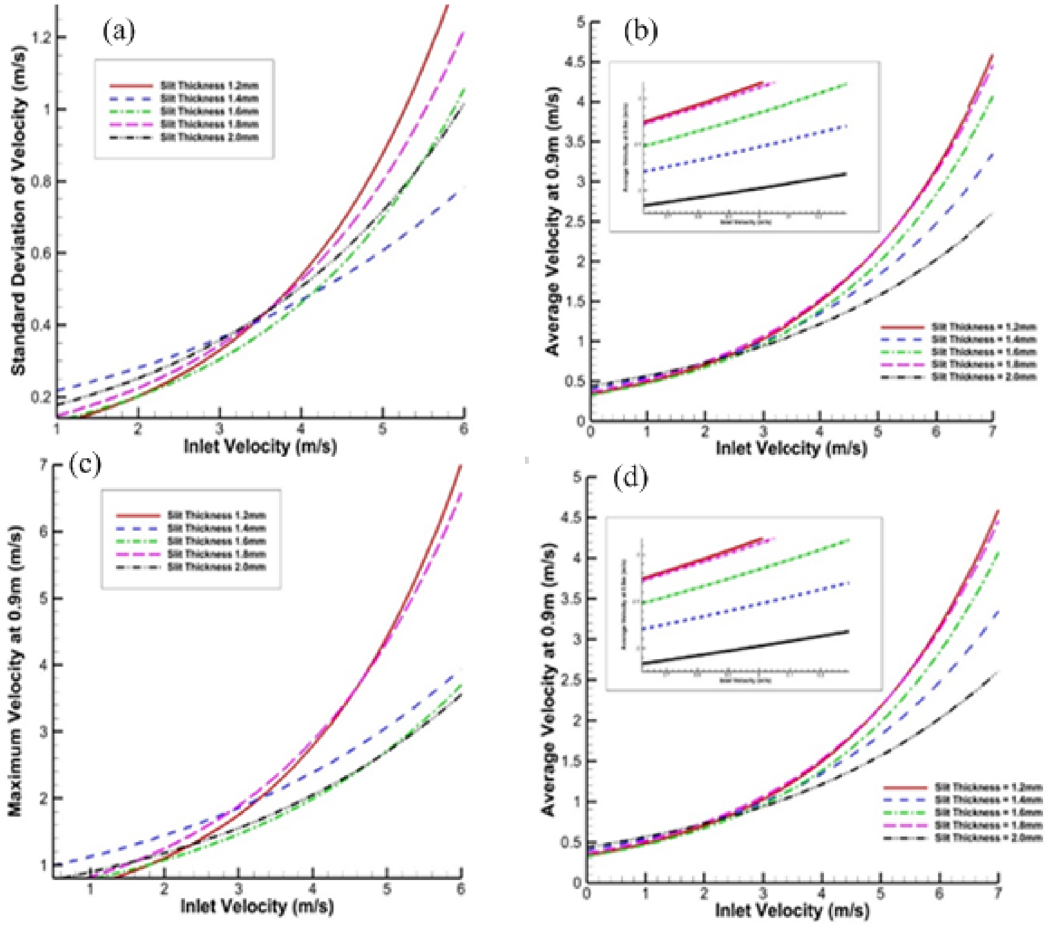

Figure 9. (**a**) Standard deviation of velocity. (**b**) Average velocity at a distance of 0.9m from the outlet slit. (**c**) Maximum velocity at a distance of 0.9 m from the outlet slit and (**d**) Maximum turbulent kinetic energy at a distance of 0.9 m from the outlet slit.

5.3. 3D Flow features

The velocity contour of the 1.2 mm had to be axis-symmetric to be accepted; if the output flow is not symmetric, it will cause discomfort to the occupants. Figure 10 shows the velocity contour, and turbulent kinetic energy of the 1.2 mm slit thickness iteration. The contour is symmetrical about the fan's horizontal axis. Figure 10 (a b) depict bladeless fans' turbulence kinetic energy and velocity magnitude flow with 1.2 mm and 2 mm slit thicknesses, respectively.

Preprints (www.preprints.org) | NOT PEER-REVIEWED | Posted: 24 November 2022 doi:10.20944/preprints202211.0459.v1

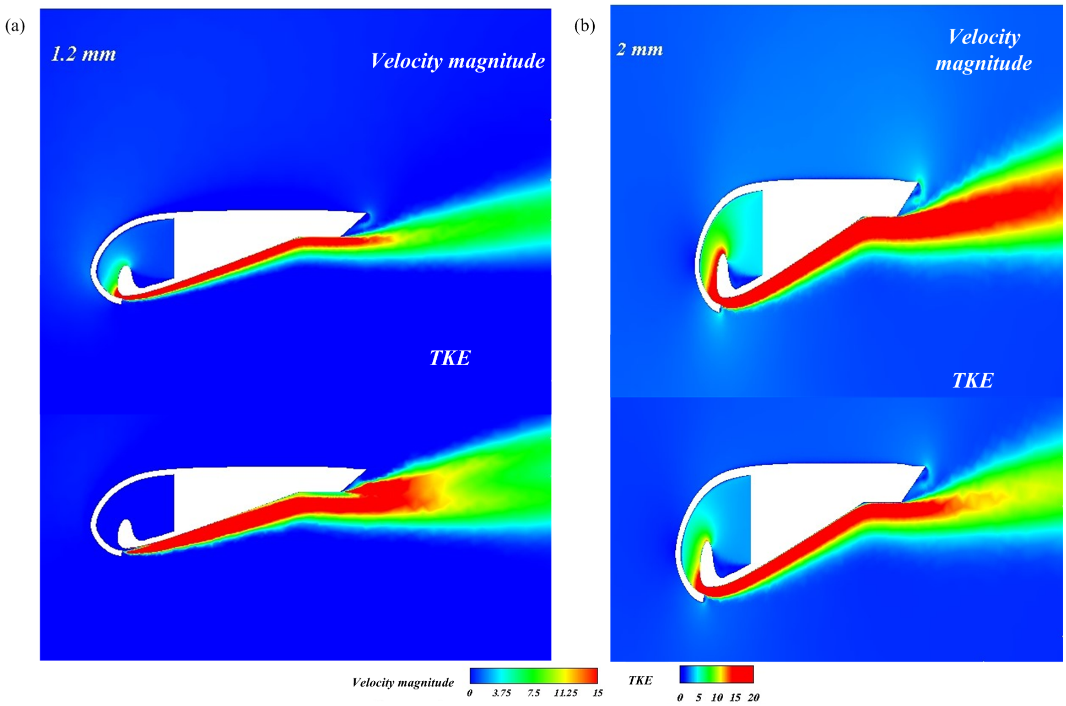

Figure 10. Velocity magnitude (m/s) and Turbulent Kinetic Energy (m^2s^{-2}) from the slit (**a**) 1.2 mm (**b**) 2 mm thickness.

Figure 11 represents the velocity contour and streamlines to depict flow amplification. Figure 12 illustrates that at planes at distances less than 0.4 m concentrated velocity profiles are formed along the circumference of the fan. This indicates that the velocity is not spread equally along the planar region, which is not ideal. At a distance of 0.4 m, the velocity distribution started to develop. From 0.9 m to 1.8 m, the velocity profile continues to develop. Finally, it attains a uniform distribution at 1.8 m, as seen in Figure 12. This observation inferred that the optimal occupant distance from the fan is 1.8 m away from the trailing edge

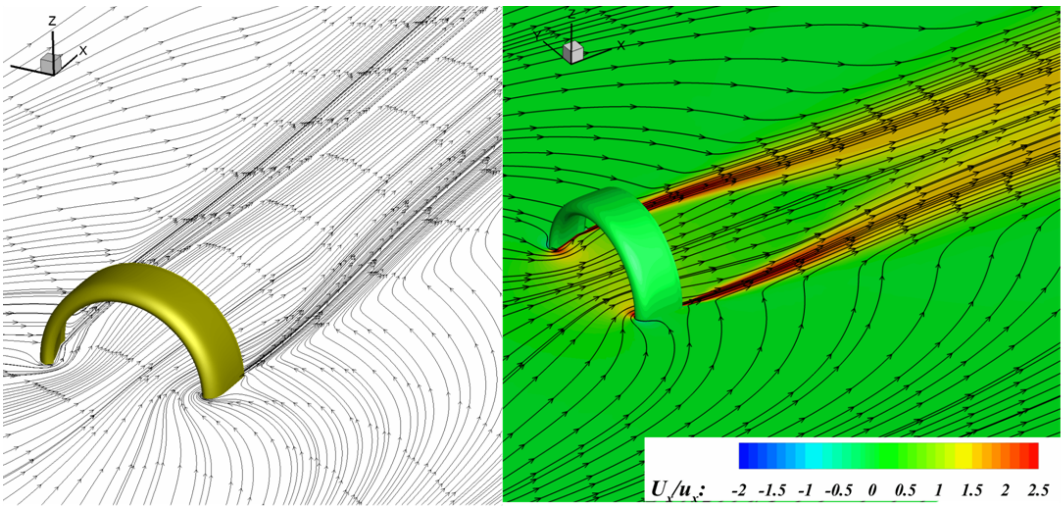

Figure 11. Streamline and Velocity contours of 1.2 mm slit thickness (V=3 m/s).

Preprints (www.preprints.org) | NOT PEER-REVIEWED | Posted: 24 November 2022 doi:10.20944/preprints202211.0459.v1

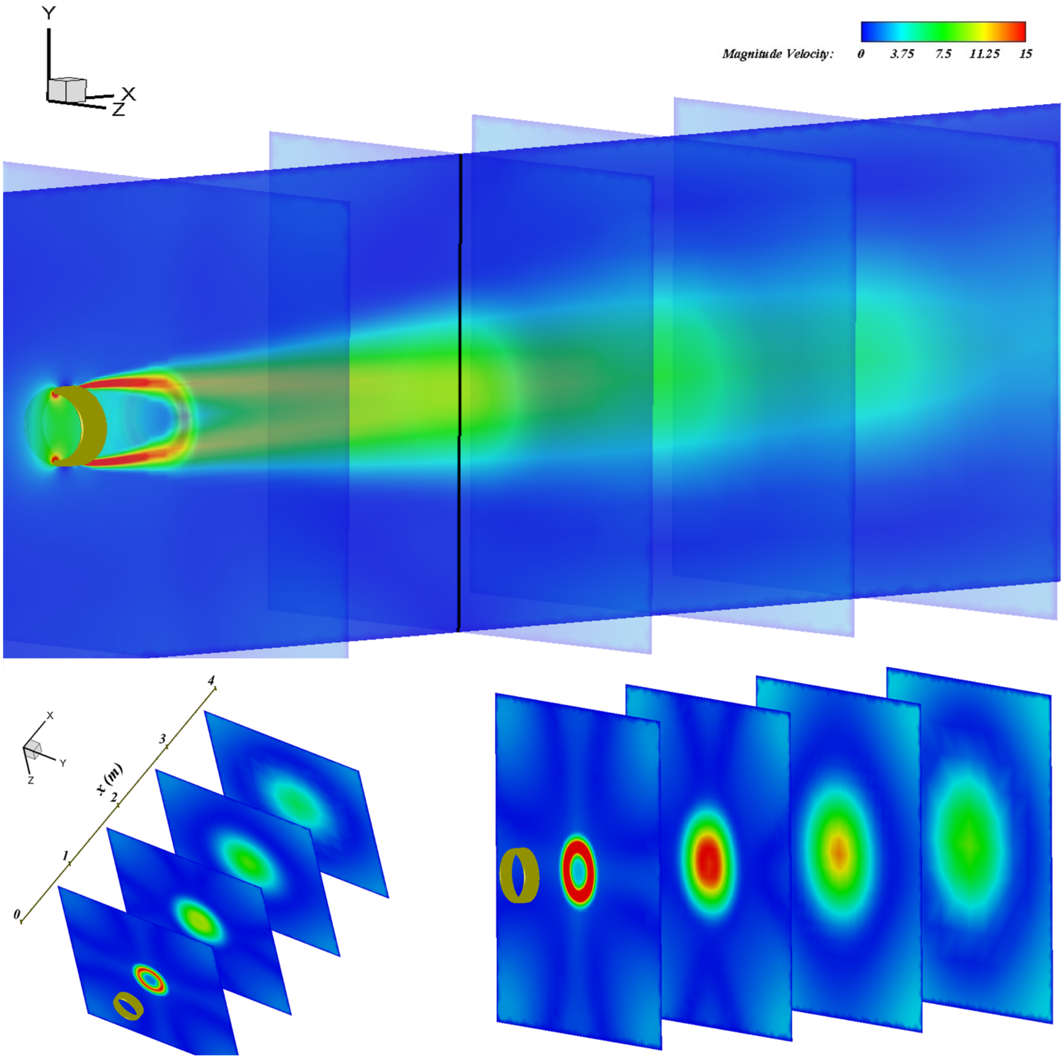

Figure 12. Perspective view of air flow at down stream of 1.2 mm slit thickness with 3 m/s inlet velocity.

Figure 13 depicts the velocity distribution of air at a certain distance from the axis. Four lines on the velocity contour plot to analyse the velocity distributions as a function of the y distance on the lines. The four curves on the graph represent each of the planes on the velocity contour diagram. The velocity at the first line (x/D=0.4 m distance from slit) shows a maximum velocity of 7.5 m/s near the centre. The second line from the left (0.9 m distance from slit) has a maximum velocity of around 4.5 m/s, and the third (1.35 m distance from slit) and fourth (1.8 m distance from slit) have velocities of 4.1 m/s and 3.7 m/s, respectively. Thus, the graph plots conclude that at a distance between 0.9 m and 1.8 m, the graph shows a lower and uniform gradient of velocity.

Preprints (www.preprints.org) | NOT PEER-REVIEWED | Posted: 24 November 2022 doi:10.20944/preprints202211.0459.v1

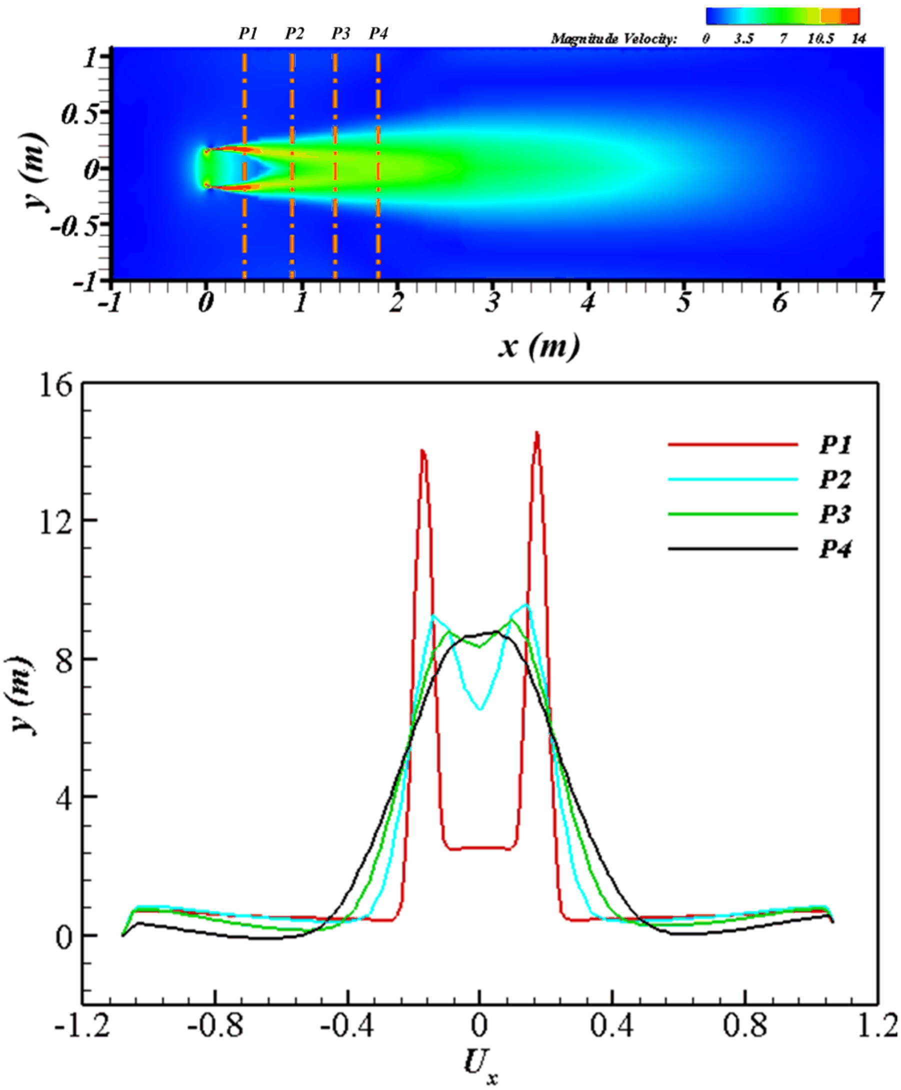

Figure 13. Perspective view of air flow at down stream of 1.2 mm slit thickness with 3 m/s inlet velocity.

The velocity profile follows a parabolic curve in bladeless fans, with the peak located at the centre. The flow develops when the velocity profile contours straighten out after converging at the parabola's vertex. The flow does not fully develop at a distance of 0.4 m from the fan, which proves that velocity remains higher closer to the circumferential area of the fan. As Figure 12 suggests, the flow becomes fully developed at a distance of around 0.9-1.35 m from the slit. While it is essential to analyse the velocity distribution of air through contours and graphs, it is also imperative to understand the direction of flow. Figure 14 represents the direction of airflow using velocity vector plots of the 2mm slit thickness iterations.

Preprints (www.preprints.org) | NOT PEER-REVIEWED | Posted: 24 November 2022 doi:10.20944/preprints202211.0459.v1

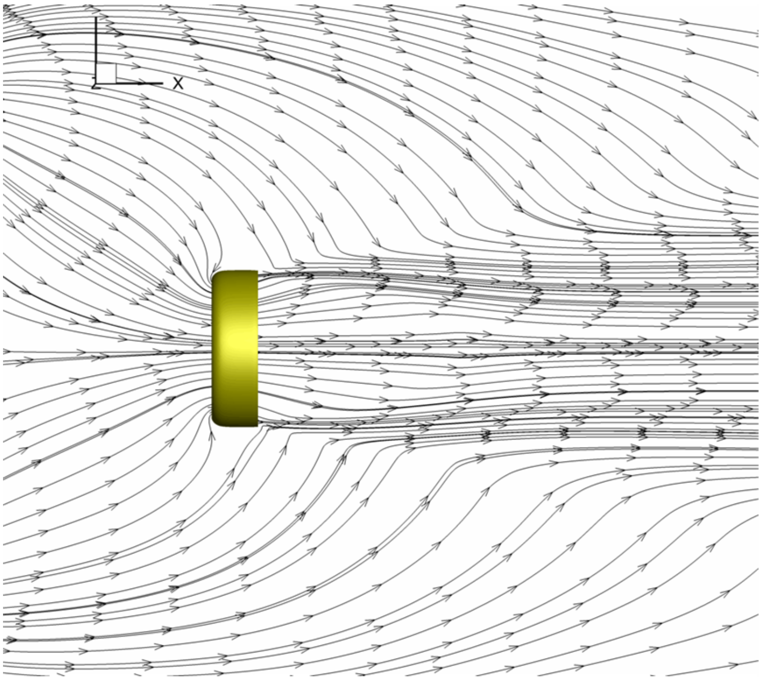

Figure 14. Velocity Vectors displaying the direction of output air in the 3D domain at a distance of 0.9 m from the fan.

Maximum velocity at different distances from the slit was observed for various slit thicknesses. The results are in the form of a plotted in Figure 15. At a very close distance from the slit, the velocity is around 20m/s. As we move from 0.1 m to 0.2 m away from the slit, the maximum velocity drops significantly from 20 m/s to 10 m/s. And from 0.2 m to 0.9 m, the velocity drops from 10m/s to nearly 5 m/s. Finally, the maximum velocity decreases at a stable rate from 5m/s to 0.143 m/s at distances greater than 1 m from the slit.

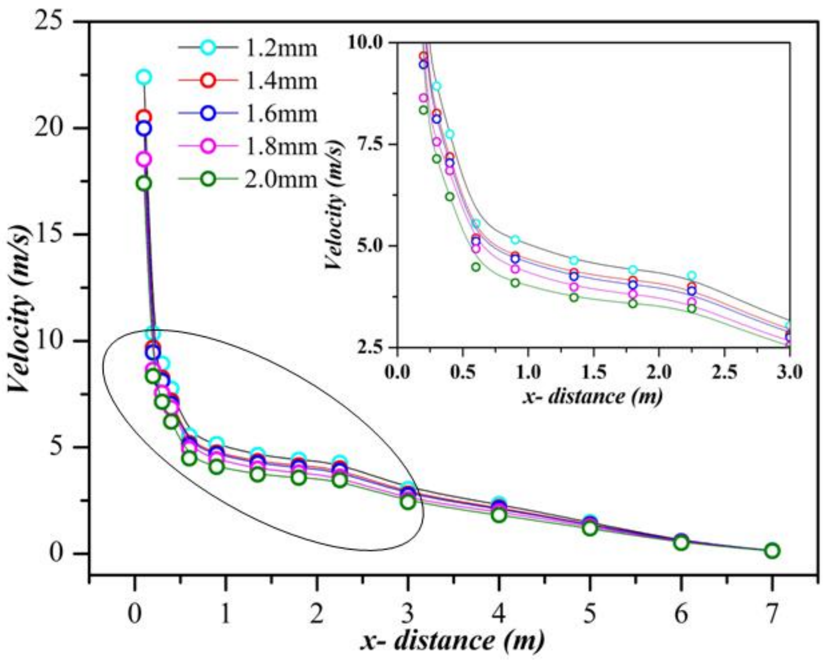

Figure 15. Maximum velocity vs distance from the slit.

The following graph shows the trend of discharge ratio to slit thickness. Since the inlet velocity is constant for the samples, the outlet velocity increases with a decrease in slit thickness. This increment of velocity due to smaller slit thicknesses increased the discharge

Preprints (www.preprints.org) | NOT PEER-REVIEWED | Posted: 24 November 2022 doi:10.20944/preprints202211.0459.v1

ratio substantially. Therefore, the case with a slit thickness of 1.2 mm showed a maximum discharge ratio of 18.784 shown in Figure 16. Another important observation is that the variation of discharge ratio for the outlet slit thickness is linearly decreasing.

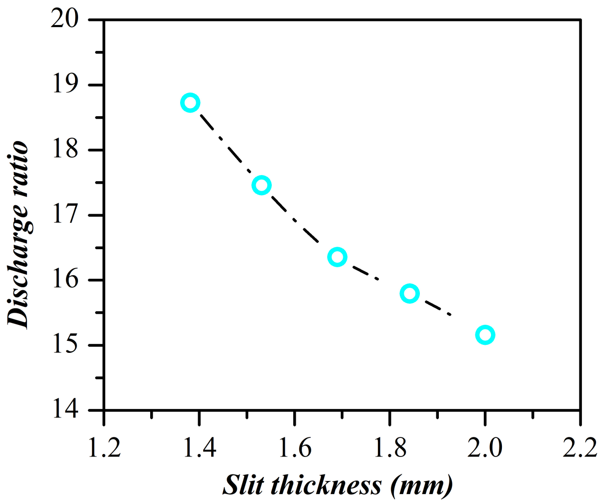

Figure 16. Slit thickness vs Discharge ratio.

5.4. Variation of outlet angle

The outlet slit angle has a significant effect on the direction of the flow of air. Variation of outlet slit angles changes the distance at which the flow fully develops. In this study, the outlet slit thickness is varied between 16 and 26 with an increment of 2 shown in Figure 17. The outlet slit thickness and inlet velocity were 1.2mm and 3m/s, respectively. These values were finalised based on previous iterations conducted on outlet slit thickness and inlet velocity variation. Increasing the outlet slit angle reduces the resultant velocity of the air coming out of the fan since a higher outlet slit angle reduces the horizontal component of air velocity. A smaller outlet slit angle increases the converging distance of the fan's velocity profile, which is undesirable. The velocity profile converging distances of the bladeless fans are plotted against various outlet angles below.

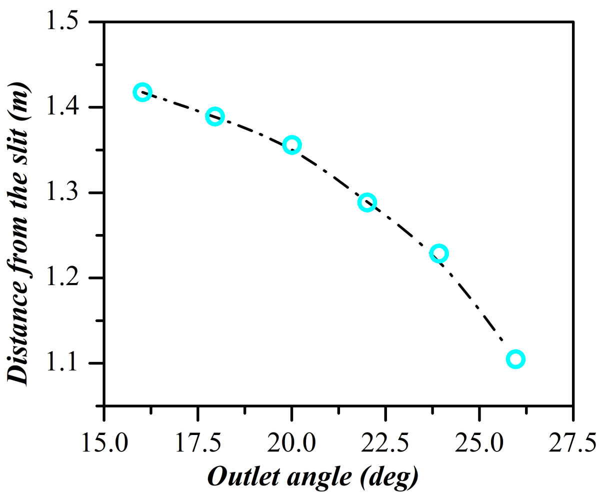

Figure 17. Converging distance for different outlet angles

The graph above shows that an outlet angle of 26 gives a convergence distance of just 1.13 m. Although 26 outlet angle creates a low convergence distance, the steep outlet angle can reduce the Coanda effect along the airfoil. To investigate this, the pressure is measured at the slit, leading-edge, and trailing edge. The graph in Figure 18 below depicts

Preprints (www.preprints.org) | NOT PEER-REVIEWED | Posted: 24 November 2022 doi:10.20944/preprints202211.0459.v1

the pressure difference between the slit, and Figure 19 shows the difference between the leading edge and the trailing edge and leading-edge pressures. Theoretically, a greater pressure difference is preferable for increasing the Coanda effect.

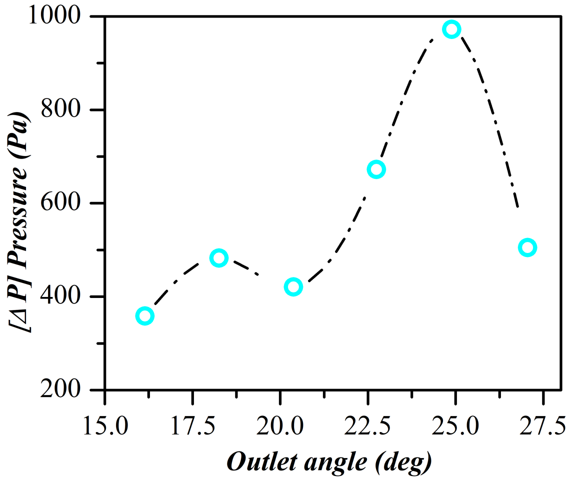

Figure 18. Pressure difference between the slit and leading edge for different outlet angle

Figure 19 inferred that the 24 outlet angle shows the greatest pressure drop across the airfoil. The other iterations show a pressure drop of around 300 to 500 Pa. Since the 24 outlet angle shows the highest pressure drop, the Coanda effect will facilitate the most. Figure 19 shows a slight pressure difference between the trailing edge and the atmosphere for the 24 outlet angle, which means there will be lesser turbulence at the front of the fan, which is suitable for its performance.

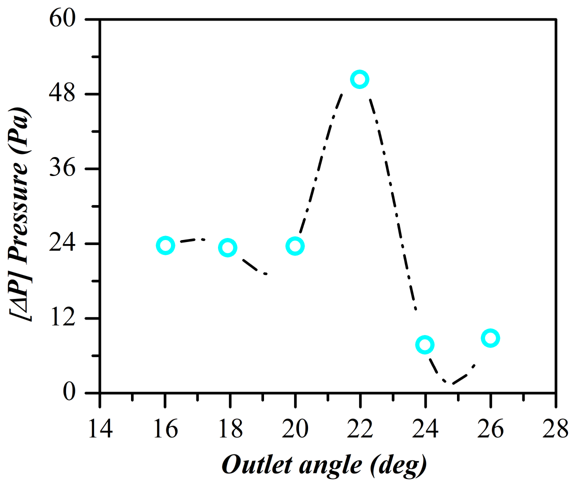

Figure 19. Pressure difference between the trailing and leading-edge for different outlet angle

6. Conclusions

This study aimed at understanding the influence of outlet slit thickness and outlet angle on the performance of the bladeless fan. The 2-dimensional analysis fortified the theoretical understanding that outlet velocity increases with a decrease in slit thickness. It was also observed that the velocity profile flattens with distance from the fan. The 3-dimensional analysis results showed that the standard deviation of all slits remains almost the same for inlet velocities under 3.3 m/s, and 1.6 mm slit thickness shows the lowest standard deviation up to 5.4 m/s inlet velocity. For inlet velocities above 2.4 m/s, the 1.2 mm slit has the highest average outlet velocity. This velocity also falls in the range of occupant comfort.

The 1.2 mm slit thickness with 3 m/s inlet velocity was considered the best for the following reasons:
i) The standard deviation is 0.25, which is small and will not cause any discomfort under operational conditions.

ii) At the velocity profile convergence distance, the outlet air velocity will be 4.85 m/s, which is comfortable.

iii) Although other iterations have higher and comparable output velocities at the target distance, the 1.2 mm slit thickness was most favourable because it consumed less energy owing to its lower input velocity.

Velocity contour plots indicated that the flow has a curved profile. The flow begins to develop at 0.9 m from the trailing edge, approximately three times the fan diameter, and fully develops at 1.8 m. The maximum velocity to distance ratio from slit plots suggested that smaller slits show higher maximum velocity throughout the upstream flow. Finally, a comparison of the discharge ratio for different slit thicknesses demonstrated that the discharge ratio decreases linearly with an increase in slit thickness. The decrement of slit thickness from 2 mm to 1.2 mm showed a 24.2% increment in the discharge ratio. The outlet angle affects the pressure difference across the airfoil. A higher-pressure difference between the slit and the trailing edge facilitates the Coanda effect. The 24-degree outlet angle showed the highest-pressure drop of 965 Pa, while the 16-outlet angle showed just a 355 Pa pressure drop, which is approximately 63% lesser. The 24 outlet does create a huge pressure difference between the leading and trailing edge, thereby reducing the chances of losses due to turbulence. In addition, the velocity profile develops 1.13 m from the trailing edge for the 26 outlet while the 16 outlet flow develops at a distance of 1.4 m.

Author Contributions:

Vedant Joshi: Modelling and simulation, data visualisation, Writing of manuscript.

Wedyn Noronha: Modelling and simulation, data visualisation, writing of manuscript.

Vinayagamurthy G: Conceptualisation, supervised the findings of the work, result interpretation, writing of manuscript.

Sivakumar R: Supervised the findings of this work, result interpretation.

KB Rajasekarababu: Experiment, CFD conceptualisation, illustration of results and writing of manuscript.

Acknowledgments: The authors of this article would like to express gratitude to the School of Mechanical Engineering (SMEC), VIT, for granting access to computational laboratories to carry out this study.

Conflicts of Interest: The authors declare that they have no competing financial interests or personal relationships that could have appeared to influence the work reported in this paper.

Abbreviations

The following abbreviations are used in this manuscript:

c_f	Skin Friction Coefficient
L	Characteristic length
R_e	Reynolds Number
TKE	Turbulence Kinetic Energy u_T
Friction velocity	
U	Freestream Velocity
y_H	Overall height of the cell adjacent to the boundary layer
y_p	Wall height adjacent cell to the centroid
y^+	Non- dimensional wall distance (value-based on turbulence model)
μ	Dynamic Viscosity
ρ	density
τ_w	wall shear stress

References

1. P.D. Gammack, F. Nicolas, K.J. Simmonds (2009), Bladeless Fan, in: Patent Application Publication. US 2009/0060710Al. United States.
2. Jafari M, Afshin H, Farhanieh B, Bozorgasareh H. Numerical aerodynamic evaluation and noise investigation of a bladeless fan. Journal of Applied Fluid Mechanics. 2014 Nov 1;8(1):133-42..
3. Jafari M, Afshin H, Farhanieh B, Bozorgasareh H. Experimental and numerical investigation of a 60cm diameter bladeless fan. Journal of Applied Fluid Mechanics. 2016 Feb 1;9(2):935-44.
4. Jafari M, Afshin H, Farhanieh B, Sojoudi A. Numerical investigation of geometric parameter effects on the aerodynamic performance of a Bladeless fan. Alexandria Engineering Journal. 2016 Mar 1;55(1):223-33..
5. Aureliano FD, Guedes LC. Computational fluid dynamics (CFD): behavioral study and optimization of the blades number of a radial fan. Procedia Manufacturing. 2019 Jan 1;38:1324-9.
6. Panigrahi DC, Mishra DP. CFD simulations for the selection of an appropriate blade profile for improving energy efficiency in axial flow mine ventilation fans. Journal of Sustainable Mining. 2014 Jan 1;13(1):15-21.
7. Jeong S, Lee J, Yoon J. Optimal nozzle design of bladeless fan using design of experiments. Transactions of the Korean Society of Mechanical Engineers A. 2017;41(8):711-9.
8. Li G, Hu Y, Jin Y, Setoguchi T, Kim HD. Influence of Coanda surface curvature on performance of bladeless fan. Journal of thermal science. 2014 Oct;23(5):422-31.
9. Sarraf C, Nouri H, Ravelet F, Bakir F. Experimental study of blade thickness effects on the overall and local performances of a controlled vortex designed axial-flow fan. Experimental Thermal and Fluid Science. 2011 May 1;35(4):684-93.
10. Mohaideen MM. Optimization of backward curved aerofoil radial fan impeller using finite element modelling. Procedia engineering. 2012 Jan 1;38:1592-8.
11. Raj D, Swim WB. Measurements of the mean flow velocity and velocity fluctuations at the exit of an FC centrifugal fan rotor.
12. Chunxi L, Ling WS, Yakui J. The performance of a centrifugal fan with enlarged impeller. Energy Conversion and Management. 2011 Aug 1;52(8-9):2902-10.